



HAL
open science

MyDEP: a new computational tool for dielectric modeling of particles and cells

Jonathan Cottet, Olivier Fabrègue, Charles Berger, François Buret, Philippe Renaud, Marie Frénéa-Robin

► **To cite this version:**

Jonathan Cottet, Olivier Fabrègue, Charles Berger, François Buret, Philippe Renaud, et al.. MyDEP: a new computational tool for dielectric modeling of particles and cells. *Biophysical Journal*, 2019, 116 (1), pp.12-18. 10.1016/j.bpj.2018.11.021 . hal-01944869

HAL Id: hal-01944869

<https://hal.science/hal-01944869v1>

Submitted on 21 Oct 2021

HAL is a multi-disciplinary open access archive for the deposit and dissemination of scientific research documents, whether they are published or not. The documents may come from teaching and research institutions in France or abroad, or from public or private research centers.

L'archive ouverte pluridisciplinaire **HAL**, est destinée au dépôt et à la diffusion de documents scientifiques de niveau recherche, publiés ou non, émanant des établissements d'enseignement et de recherche français ou étrangers, des laboratoires publics ou privés.



Distributed under a Creative Commons Attribution - NonCommercial 4.0 International License

MyDEP: a new computational tool for dielectric modeling of particles and cells

Jonathan Cottet^{1,2}, Olivier Fabregue¹, Charles Berger¹, François Buret¹, Philippe Renaud² and Marie Frénéa-Robin¹

¹ *Univ Lyon, Ecole Centrale de Lyon, Université Claude Bernard Lyon 1, INSA Lyon, CNRS, Ampère, F-69130, Ecully, France*

² *École Polytechnique Fédérale de Lausanne, EPFL-STI-IMT-LMIS4, Station 17, CH-1015 Lausanne, Switzerland*

Corresponding author: Jonathan Cottet
e-mail: jonathan.cottet@epfl.ch

Keywords: Dielectrophoresis, Cell trapping, Microfluidics, Bottom-up assembly

ABSTRACT

Dielectrophoresis (DEP) and electrorotation (ROT) are two electrokinetic phenomena exploiting non-uniform electric fields to exert a force or torque on biological particles suspended in liquid media. They are widely used in lab-on-chip devices for the manipulation, trapping, separation and characterization of cells, microorganisms and other particles. The DEP force and ROT torque depend on the respective polarizabilities of the particle and medium, which in turn depend on their dielectric properties and on the field frequency. In this paper, we present a new software, MyDEP, which implements several particle models based on concentric shells with adjustable dielectric properties. This tool enables to study the variation in DEP and ROT spectra according to different parameters such as the field frequency and medium conductivity. Such predictions of particle behavior are very useful for choosing appropriate parameters in DEP experiments. The software also enables to study the homogenized properties of spherical or ellipsoidal multishell particles and provides a database containing published cell properties. Equivalent electrical conductivity and relative permittivity of the cell alone and in suspension can be calculated. The software also offers the possibility to create graphs of the evolution of the crossover frequencies with the electric field frequency. These graphs can be directly exported from the software.

INTRODUCTION

The term “dielectrophoresis” was first introduced by Pohl in 1951 (1) to describe the motion of dielectric particles due to interaction with a non-uniform electric field. Depending on the frequency of the applied field and on the dielectric properties of the particle and its immersion medium, different polarization mechanisms come into play, the main mechanisms being related to the formation of a double electric layer at the particle/liquid interface and to charge accumulation at interfaces between media of different electrical properties (Maxwell-Wagner interfacial polarization effect) (2). The force resulting from the interaction between the induced dipole moment \mathbf{m} and the field gradient is expressed by:

$$\mathbf{F}_{\text{DEP}} = -\nabla U_{El} = (\mathbf{m} \cdot \nabla) \mathbf{E} \quad (1)$$

where U_{El} refers to the electric potential energy and \mathbf{E} to the electric field.

For a spherical particle of radius r_{ext} , the induced dipolar moment is given by:

$$\mathbf{m} = 4\pi\epsilon_m\epsilon_0 CM(f)r_{ext}^3 \mathbf{E} \quad (2)$$

where $CM(f)$ is the Clausius-Mossotti factor:

$$CM(f) = \frac{\epsilon_p^* - \epsilon_m^*}{\epsilon_p^* + 2\epsilon_m^*} \quad (3)$$

ϵ_p^* and ϵ_m^* refer to the complex permittivities of particle and medium, which depend on their respective electrical conductivities and relative permittivities and on the field angular frequency ω :

$$\epsilon_i^* = \epsilon_i\epsilon_0 - j\frac{\sigma_i}{\omega} \quad (4)$$

where ε_i is the relative permittivity, ε_0 the vacuum permittivity, σ_i the electrical conductivity and $\omega = 2\pi f$ with f the frequency.

Development of Eq. 1 leads to the expression of the generalized time-averaged DEP force (3):

$$\mathbf{F}_{\text{DEP}} = 2\pi\varepsilon_m\varepsilon_0r_{\text{ext}}^3 \left(\text{Re}[CM(f)]\nabla E_{\text{RMS}}^2 + \text{Im}[CM(f)](E_x^2\nabla\phi_x + E_y^2\nabla\phi_y + E_z^2\nabla\phi_z) \right) \quad (5)$$

where ϕ_x , ϕ_y and ϕ_z are the phase shifts of the field components in the Cartesian coordinates.

Conventional Dielectrophoresis

If the electric field applied is stationary, Eq. 5 simplifies to:

$$\mathbf{F}_{\text{cDEP}} = 2\pi\varepsilon_m\varepsilon_0r_{\text{ext}}^3 \text{Re}[CM(f)]\nabla E_{\text{RMS}}^2 \quad (6)$$

This phenomenon is sometimes referred to as “conventional dielectrophoresis”, abbreviated cDEP. The force depends on the gradient of the squared electric field intensity and exists only in the presence of a non-uniform electric field. It is proportional to the volume of the particle, as well as to the real part of the Clausius-Mossotti factor, $\text{Re}[CM(f)]$. This term, reflecting the polarizability contrast between the particle and its immersion medium, also determines the direction of the force:

- When the particle is more polarizable than its immersion medium ($\text{Re}[CM(f)] > 0$), the force acts in the gradient direction and therefore drives the particle towards areas of maximum field intensity. This corresponds to *positive dielectrophoresis* (pDEP).

- On the contrary, when the particle is less polarizable than its immersion medium ($Re[CM(f)] < 0$), the force moves the particle against the gradient, towards the regions of minimum field intensity, which is referred to as *negative dielectrophoresis* (nDEP).

Electrorotation

While conventional dielectrophoresis is based on the use of stationary electric fields, electrorotation, abbreviated ROT, induces a rotary motion on a polarizable particle exposed to a rotating field. This technique was developed in the 1980s by Arnold and Zimmermann (4), who proposed to use a four-pole electrode structure to generate the field by applying 90° phase-shifted signals between two adjacent electrodes.

When a polarizable particle is suspended in a rotating electric field, a dipole forms and should rotate synchronously with the field. In practice, when the angular frequency of the field is sufficiently high, the dipolar relaxation time is too long to allow this synchronism. The temporal shift (or phase delay) between the dipole and the field results in a torque exerted on the particle, of expression:

$$\langle \Gamma_{EL} \rangle = \mathbf{m} \times \mathbf{E} = -4\pi r_{ext}^3 \varepsilon_m \varepsilon_0 \text{Im}[CM(f)] E^2 \mathbf{e}_z \quad (7)$$

where \mathbf{e}_z represents the unit vector normal to the electrode plane and $CM(f)$ the Clausius-Mossotti factor (cf. Eq. 3).

As the particle rotates, it experiences a resistive viscous torque from the surrounding fluid of expression (5):

$$\langle \Gamma_{\eta} \rangle = -8\pi \eta r_{ext}^3 \Omega_0 \mathbf{e}_z \quad (8)$$

where η is the dynamic viscosity of the medium and Ω_0 is the constant angular velocity of the particle.

At the equilibrium between induced torque and resistive viscous torque, the rotation rate for a spherical particle is given by:

$$\Omega(\omega) = -\frac{\epsilon_0\epsilon_m}{2\eta} \text{Im}[CM(f)]E^2 \quad (9)$$

The minus sign indicates that the particle rotates against the field direction for $\text{Im}[CM(f)] > 0$. Otherwise the direction of rotation is with the field. Curve fitting procedures may be used to obtain the dielectric parameters of a cell, by minimizing the deviation between the experimental ROT spectrum (plot of the rotation rate with respect to the field frequency) and the theoretical spectrum predicted by the appropriate multi-shell model.

Travelling-Wave Dielectrophoresis (TWD)

The Travelling-Wave Dielectrophoresis force, abbreviated TWD, acts on a particle subjected to a travelling electric field. It is related to the phase non-uniformity of the electric field and arises from the interaction of the travelling field with the phase-lagging component of the induced dipole moment. Such a field can be produced by planar electrodes arranged in rows and driven by a polyphase AC voltage. TWD is therefore an analogue of ROT, Eq 5 remains the same, but with electrodes arranged in line, rather than in a circle. The resulting translational force propels the particle along the electrodes, with or against the field direction, depending on whether $\text{Im}[CM(f)]$ is negative or positive, respectively. In practice, cDEP and TWD effects can be observed simultaneously: while the particle translates, it is either pushed above the electrodes (nDEP) or attracted onto them (pDEP), depending on the sign of $\text{Re}[CM(f)]$ (6).

MyDEP Software

Before performing experiments in the lab with DEP, it is useful to predict the particle and cell responses to the electric field. This requires knowledge of particles or cells properties, which can be obtained from the literature, and implementation of equations related to the particle model.

MyDEP is a computational software, programmed in Java, aiming to study dielectrophoretic behavior of particles and cells in a suspended medium. More precisely the software can calculate and display the Clausius-Mossotti factor (real and imaginary parts) used in DEP for different conditions (medium, frequency range, model of particle). It can also calculate the equivalent permittivities and conductivities of particles alone and in suspension in a medium thanks to the Maxwell-Garnett and Hanai equations. Graphs representing crossover frequencies vs electrical conductivity of the medium are also available.

Cell modeling

Most particles, and especially biological cells, are not homogeneous. It is therefore mandatory to model the different layers that constitute them (cell membrane and cytoplasm in particular). Calculating the Clausius-Mossotti factor requires to successively calculate the equivalent permittivities of the inner layers to obtain a homogeneous equivalent particle. The different models implemented in MyDEP are: “homogeneous particle”, “single-shell”, “two-shell”, “three-shell” and “four-shell” are presented in FIGURE 1.

For a cell modeled with a “single-shell” model composed of a cytoplasm surrounded by a cell membrane, the equivalent complex permittivity (7) is:

$$\epsilon_{eq}^* = \epsilon_{cm}^* \frac{\left(\frac{r_{ext}}{r_{ext} - th_{cm}}\right)^3 + 2\left(\frac{\epsilon_{cp}^* - \epsilon_{cm}^*}{\epsilon_{cp}^* + 2\epsilon_{cm}^*}\right)}{\left(\frac{r_{ext}}{r_{ext} - th_{cm}}\right)^3 - \left(\frac{\epsilon_{cp}^* - \epsilon_{cm}^*}{\epsilon_{cp}^* + 2\epsilon_{cm}^*}\right)} \quad (10)$$

The formulation of the complex permittivity for ellipsoids can be found in (8).

Cell suspension

In the presence of particles, the effective permittivity of the suspension ϵ_{mix}^* depends on the volume fraction ϕ occupied by the particles. It is given by the Maxwell-Garnett mixing equation if the volume fraction $\phi < 0.1$

$$\frac{\epsilon_{mix}^* - \epsilon_m^*}{\epsilon_{mix}^* + 2\epsilon_m^*} = \phi \frac{\epsilon_p^* - \epsilon_m^*}{\epsilon_p^* + 2\epsilon_m^*} \quad (11)$$

which is equivalent, according to (9), to the direct formulation:

$$\epsilon_{mix}^* = \epsilon_m^* \left(1 + 3\phi \frac{\frac{\epsilon_p^* - \epsilon_m^*}{\epsilon_p^* + 2\epsilon_m^*}}{1 - \phi \frac{\epsilon_p^* - \epsilon_m^*}{\epsilon_p^* + 2\epsilon_m^*}} \right) \quad (12)$$

or by the Hanai equation (10), theoretically up to $\phi < 0.8$ (11, 12):

$$\left(\frac{\epsilon_{mix}^* - \epsilon_p^*}{\epsilon_m^* - \epsilon_p^*}\right) \left(\frac{\epsilon_m^*}{\epsilon_p^*}\right)^{1/3} = 1 - \phi \quad (13)$$

Unfortunately, there is no direct expression for the calculation of ϵ_{mix}^* and the value can therefore be obtained either by solving the cubic equation or by numerical integration with the difference equation of the Hanai equation. The later has been implemented in MyDEP, with the possibility to choose the number of increments. The methodology can be found in (13, 14).

Software for dielectric modeling

In 1991, Irimajiri and al. (14) published a software for dielectric modeling of particles in suspension called “IMPEDANCE ANALYSIS mini”, programmed in BASIC. Unfortunately, this program is not available anymore.

Dielectric modeling of particles behavior is often done in MATLAB (2, 3) and some authors have proposed MATLAB-based programs that are available (15). Those programs are however limited in terms of functionalities implemented, platform dependent and may lack stability through the different releases of MATLAB and require an access to MATLAB. For those reasons a multiplatform, executable and user-friendly program is needed. This software is intended to be used by both the dielectrophoresis community and for teaching activities. It does not require any prior knowledge of the dielectrophoresis equations.

MATERIALS AND METHODS

The software MyDEP is written in Java using the swing API and is freely available as a standalone .jar file for Windows, Mac or Linux at <http://doi.org/10.5281/zenodo.1321928>. The installation of Java (also known as the Java Runtime Environment or JRE) is required (<https://java.com/en/download>). The software version number as well as the recommended java version are available on the website <https://mydepsoftware.github.io>, under the “Getting Started” menu (item “Installation and system requirements”).

A local database is embedded within the application using the SQL database engine SQLite. The Java Database Connectivity (JDBC) API was used to interact with SQLite.

The static website hosted on GitHub Pages was build using Jekyll. A link to the website is available in the software under the “Help” menu (item “Online resources”).

RESULTS AND DISCUSSION

Database

MyDEP allows the user to specify the electrical as well as the geometrical parameters of the investigated particle. No prior knowledge of the equations behind is required to use the software, which makes it interesting for users non-familiar with DEP. A database compiling information from the literature is provided to help the user to start with already existing data. The user can also enrich the database with new information. A local database is embedded within the application using the SQL database engine SQLite. The Java Database Connectivity (JDBC) API was used to interact with SQLite. The provided database contains for each set of data the name of the model, the authors, the title of the article, the journal where it was published, the year of publication as well as the DOI or URL to help the users to identify where the model they are using is coming from. An example of the database explorer is displayed in FIGURE 2.

CM factor

MyDEP allows the user to display different graphs linked to the dielectric properties of particles and cells. Real and imaginary parts of the Clausius-Mossotti factor can be displayed in the interface. Users can get values about the displayed curves in the “Results” panel. In particular the values of the crossover frequencies, corresponding to the frequencies at which $Re[CM(f)] = 0$, are directly accessible as well as the frequencies of the minimum and maximum of $Im[CM(f)]$. This graph can be used to determine the direction of the DEP force. As shown in FIGURE 3, viable and non-viable yeast cells have a different behavior for the same medium

conductivity, $\sigma_m = 7.8 \text{ mS/m}$. The DEP force, which is proportional to $\text{Re}[CM(f)]$, is always higher in magnitude for the viable yeast cells.

Parameter sweep

All the parameters of the medium and of the different models can be swept linearly or logarithmically between two values. FIGURE 4 illustrates the graph generated by a logarithmic sweep on ten values of σ_m for Jurkat cells (17). The more the electrical conductivity increases, the lower the initial values of the $\text{Re}[CM(f)]$ and the shorter the frequency range where Jurkat cells experience pDEP. As σ_m increases, the frequencies of the maximum and minimum of $\text{Im}[CM(f)]$ are shifted to higher values up to the point where $\text{Im}[CM(f)]$ keeps a positive value.

Cell separation

Depending on their dielectric properties, different cell types can be separated. FIGURE 5 illustrates that HEK cells (18) and MCF7 (19) have different responses to the electric field with the frequency. The crossover frequency, transition from the nDEP regime to the pDEP regime, are respectively 169 kHz and 65 kHz for the HEK and MCF7 cells in the specified medium. These two cell populations can be separated based on their electrical properties between these frequencies. In particular at 100 kHz (vertical blue line in FIGURE 5) HEK cells experience nDEP contrary to MCF7 cells, which experience pDEP.

Conductivity and permittivity of cell and suspension

FIGURE 6, FIGURE 7 and FIGURE 8 illustrate how cells and medium properties influence the properties of the suspension. In each of those figures the orange dotted line corresponds to

the properties of the medium alone and the blue solid line to the homogenized properties of a HEK cell. The green dashed line corresponds to the properties of the suspension at a specific volume fraction, $\phi = 0.3$ for those figures.

Crossover frequencies

Crossover frequencies correspond to the frequencies at which $Re[CM(f)] = 0$. It corresponds to the transition from a nDEP regime to a pDEP regime and vice versa. For each electrical conductivity σ_m , this value might differ. FIGURE 9 illustrates the evolution of the crossover frequencies with σ_m for a Jurkat cell. In this figure, the lower crossover, in blue, corresponds to the transition from nDEP to pDEP and the upper crossover frequency, in orange, to the transition from pDEP to nDEP. At approximately $\sigma_m = 0.392 S/m$, there is only one crossover frequency point which means that, at a higher conductivity, cells only experience nDEP. Crossover frequencies are commonly used as a discriminatory factor between different cell types

Graph export

All the graph generated in MyDEP are fully editable. The font style and size, the color, the legend content, the curve style and size can all be adjusted directly in the interface. The export menu enables the user to directly generate the displayed graph as an image file with the possibility to tune the size and resolution as well as the file format. A CSV file can be generated if additional data processing is required and not already available in the MyDEP software.

CONCLUSIONS

MyDEP offers a new software alternative aimed at both DEP specialists and beginners. The software, delivered with a database compiling data from the literature, which can be updated automatically, aims at centralizing the electrical properties published in the literature and making them easily accessible to generate graphs. MyDEP also offers the possibility to import the user's own data points to compare them to different cell models. Future developments of MyDEP will be towards parameters extraction from the user's own dataset and to impedance calculation.

SUPPORTING MATERIAL

Supporting Materials and Methods containing theoretical calculations and formulas used in MyDEP are available.

Authors contributions

J.C. created the software and implemented the first version in MATLAB. O.F. and J.C. implemented the software in Java. C.B. helped with the database. F.B., P.R. and M.F.-R. supervised the research. J.C. and M.F.-R. wrote the article and built the GitHub page. All authors approved the final version of the manuscript.

Acknowledgments

The authors would like to thank the Koji Asami and Marc Castellarnau for the data provided to test the software. The Ampere lab would like to acknowledge support from INSERM (Plan Cancer, Physicancer Program, Dynamo project). The authors also acknowledge the support of the Programme d'Avenir Lyon Saint-Etienne (PALSE mobility grant), the labex iMUST (ANR-10-LABX-0064/ANR-11-IDEX-0007) from University of Lyon as well as the Doctoral school 160 EEA of the University of Lyon for the mobility grant allocated.

References

1. Pohl, H. A. 1951. The Motion and Precipitation of Suspensoids in Divergent Electric Fields. *J. Appl. Phys.* 22(7):869-871.
2. Pethig, R. R. 2017. *Dielectrophoresis: Theory, methodology and biological applications.* John Wiley & Sons.
3. Hughes, M. P. 2002. *Nanoelectromechanics in engineering and biology.* CRC, Boca Raton, Fla.; London.
4. Arnold, W. M., and U. Zimmermann. 1988. Electro-Rotation - Development of a Technique for Dielectric Measurements on Individual Cells and Particles. *J. Electrostatics* 21(2-3):151-191.
5. Lei, U., C. Y. Yang, and K. C. Wu. 2006. Viscous torque on a sphere under arbitrary rotation. *Appl. Phys. Lett.* 89(18).
6. Jones, T. B. 2003. Basic theory of dielectrophoresis and electrorotation. *IEEE Eng Med Biol Mag* 22(6):33-42.
7. Gascoyne, P. R. C., F. F. Becker, and X. B. Wang. 1995. Numerical-Analysis of the Influence of Experimental Conditions on the Accuracy of Dielectric Parameters Derived from Electrorotation Measurements. *Bioelectrochem. Bioenerget.* 36(2):115-125.
8. Kakutani, T., S. Shibatani, and M. Sugai. 1993. Electrorotation of non-spherical cells: Theory for ellipsoidal cells with an arbitrary number of shells. *Bioelectrochem. Bioenerget.* 31(2):131-145.
9. Sihvola, A. H., and J. A. Kong. 1988. Effective permittivity of dielectric mixtures. *IEEE Transactions on Geoscience and Remote Sensing* 26(4):420-429.
10. Hanai, T. 1960. Theory of the dielectric dispersion due to the interfacial polarization and its application to emulsions. *Kolloid-Zeitschrift* 171(1):23-31. journal article.
11. Hanai, T. 1968. Electrical properties of emulsions. *Emulsion science.* P. Sherman, editor. Academic Press, London, pp. 353-478.
12. Hanai, T., T. Imakita, and N. Koizumi. 1982. Analysis of Dielectric Relaxations of W/O Emulsions in the Light of Theories of Interfacial Polarization. *Colloid. Polym. Sci.* 260(11):1029-1034.
13. Hanai, T., K. Asami, and N. Koizumi. 1979. Dielectric theory of concentrated suspension of shell-spheres in particular reference to the analysis of biological cell suspensions. *Bulletin of the Institute for Chemical Research, Kyoto University* 57(4):297-305.
14. Irimajiri, A., T. Suzaki, K. Asami, and T. Hanai. 1991. Dielectric modeling of biological cells. Models and algorithm. *Bull. Inst. Chem. Res., Kyoto University* 69:421-438.
15. Erdem, N., Y. Yıldızhan, and M. Elitaş. 2017. A numerical approach for dielectrophoretic characterization and separation of human hematopoietic cells. *International Journal of Engineering Research & Technology (IJERT)* 6(4):1079-1082.
16. Talary, M. S., J. P. H. Burt, J. A. Tame, and R. Pethig. 1996. Electromanipulation and separation of cells using travelling electric fields. *Journal of Physics D-Applied Physics* 29(8):2198-2203.
17. Reichle, C., T. Schnelle, T. Muller, T. Leya, and G. Fuhr. 2000. A new microsystem for automated electrorotation measurements using laser tweezers. *Biochimica Et Biophysica Acta-Bioenergetics* 1459(1):218-229.
18. Zimmermann, D., M. Kiesel, U. Terpitz, A. Zhou, R. Reuss, J. Kraus, W. A. Schenk, E. Bamberg, and V. L. Sukhorukov. 2008. A combined patch-clamp and electrorotation study of the

voltage- and frequency-dependent membrane capacitance caused by structurally dissimilar lipophilic anions. *J. Membr. Biol.* 221(2):107-121.

19. Henslee, E. A., M. B. Sano, A. D. Rojas, E. M. Schmelz, and R. V. Davalos. 2011. Selective concentration of human cancer cells using contactless dielectrophoresis. *Electrophoresis* 32(18):2523-2529.

Figure caption

FIGURE 1 Illustration of the different spherical and ellipsoidal cell and particle models implemented in the interface. All the models “homogeneous sphere”, “single-shell”, “two-shell” and “three-shell” are illustrated with an example. The implemented “four-shell” model is not illustrated here.

FIGURE 2 Overview of the database explorer (Search) from MyDEP. A click on the desired element from the literature shows the values associated in the interface.

FIGURE 3 Example of $Re[CM(f)]$ and $Im[CM(f)]$ for viable and non-viable yeast cells suspended in a low conductivity medium ($\sigma_m = 7.8 \text{ mS/m}$, $\epsilon_m = 78$). Data from (16). The black line represents the baseline at 0.

FIGURE 4 Example of the evolution of $Re[CM(f)]$ and $Im[CM(f)]$ with a logarithmic sweep on ten values of σ_m from 1 mS/m to 1.6 S/m for a Jurkat cell. Data from (17). The black line represents the baseline at 0.

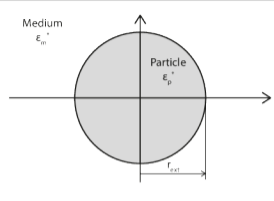
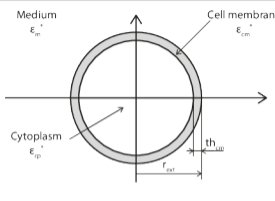
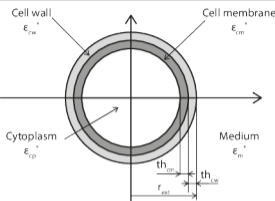
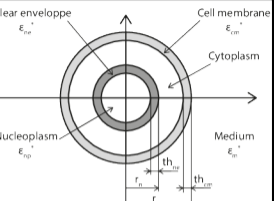
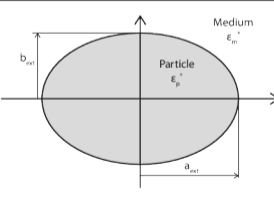
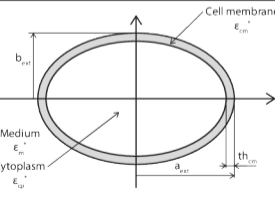
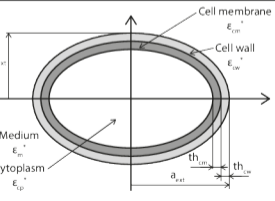
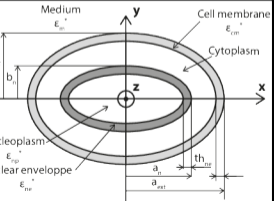
FIGURE 5 Example of the different $Re[CM(f)]$ for a HEK cell (18) and a MCF-7 cell (19) in a medium with $\sigma_m = 50 \text{ mS/m}$. The crossover frequencies are respectively 169 kHz and 65kHz. These two cell populations can be separated based on their electrical properties at 100 kHz (vertical blue line).

FIGURE 6 ϵ_{eq} , ϵ_m and ϵ_{mix} corresponding to respectively the equivalent relative permittivity of a HEK cell, the relative permittivity of the suspension medium and the equivalent relative permittivity of the suspension of HEK cells at a volume fraction $\phi=0.3$ (implemented using the Hanai methodology). $\sigma_m = 0.156 \text{ S/m}$.

FIGURE 7 σ_{eq} , σ_m and σ_{mix} corresponding to respectively the equivalent electrical conductivity of a HEK cell, the electrical conductivity of the suspension medium and the equivalent electrical conductivity of the suspension of HEK cells at a volume fraction $\phi=0.3$ (implemented using the Hanai methodology). $\sigma_m = 0.156 \text{ S/m}$.

FIGURE 8 $|\epsilon_{eq}^*|/\epsilon_0$, $|\epsilon_m^*|/\epsilon_0$ and $|\epsilon_{mix}^*|/\epsilon_0$ corresponding to respectively the modulus of the equivalent complex relative permittivity of a HEK cell, the modulus of the complex relative permittivity of the medium and the modulus of the equivalent complex relative permittivity of the HEK cells in suspension in the medium at a volume fraction $\phi=0.3$ (implemented using the Hanai methodology). $\sigma_m = 0.156 \text{ S/m}$.

FIGURE 9 Evolution of the crossover frequencies for a Jurkat cell for 50 conductivities logarithmically spaced between 1 mS/m and 0.5 S/m.

	Homogeneous Particle	Single-shell	Two-shell	Three-shell
Sphere	 <p>Medium ϵ_m^*</p> <p>Particle ϵ_p^*</p> <p>r_{ext}</p> <p>(ex: Polystyrene bead)</p>	 <p>Medium ϵ_m^*</p> <p>Cell membrane ϵ_{cm}^*</p> <p>Cytoplasm ϵ_{cp}^*</p> <p>r_{ext}</p> <p>th_{cm}</p> <p>(ex: Jurkat cell)</p>	 <p>Cell wall ϵ_{cw}^*</p> <p>Cell membrane ϵ_{cm}^*</p> <p>Cytoplasm ϵ_{cp}^*</p> <p>Medium ϵ_m^*</p> <p>r_{ext}</p> <p>th_{cm}</p> <p>th_{cw}</p> <p>(ex: Yeast cell)</p>	 <p>Nuclear envelope ϵ_{np}^*</p> <p>Cell membrane ϵ_{cm}^*</p> <p>Cytoplasm ϵ_{cp}^*</p> <p>Nucleoplasm ϵ_{np}^*</p> <p>Medium ϵ_m^*</p> <p>r_{ext}</p> <p>r_n</p> <p>th_{cp}</p> <p>th_{cm}</p> <p>(ex: Human B lymphocytes)</p>
Ellipsoid	 <p>Medium ϵ_m^*</p> <p>Particle ϵ_p^*</p> <p>b_{ext}</p> <p>a_{ext}</p> <p>(ex: Polystyrene bead)</p>	 <p>Cell membrane ϵ_{cm}^*</p> <p>Medium ϵ_m^*</p> <p>Cytoplasm ϵ_{cp}^*</p> <p>a_{ext}</p> <p>b_{ext}</p> <p>th_{cm}</p> <p>(ex: Normal tonsillar B cell)</p>	 <p>Cell membrane ϵ_{cm}^*</p> <p>Cell wall ϵ_{cw}^*</p> <p>Medium ϵ_m^*</p> <p>Cytoplasm ϵ_{cp}^*</p> <p>a_{ext}</p> <p>b_{ext}</p> <p>th_{cm}</p> <p>th_{cw}</p> <p>(ex: E. Coli K38)</p>	 <p>Medium ϵ_m^*</p> <p>Cell membrane ϵ_{cm}^*</p> <p>Cytoplasm ϵ_{cp}^*</p> <p>Nucleoplasm ϵ_{np}^*</p> <p>Nuclear envelope ϵ_{np}^*</p> <p>Medium ϵ_m^*</p> <p>a_{ext}</p> <p>b_{ext}</p> <p>a_n</p> <p>th_{cp}</p> <p>th_{cm}</p> <p>(E Coli: double-shelled prolate)</p>

File Database Interface Graph Tools Help

Medium

Save Delete Create View

Water

σ_m 1.00E-3 S/m ϵ_m 78

Volume fraction Φ 0.3 Maxwell Hanai

Frequencies

f_{start} 1000 Hz

f_{stop} 1.0E9 Hz

nb_{points} 10000

Model

Homogeneous Particle Single-shell Two-shell Three-shell Four-shell

Save Delete Create View references

HEK 293 cell line

Geometry

Radius (μm) Sphere Ellipsoid Randomly oriented

Particle r_{ext} 7.5 a_{ext} 7.5 b_{ext} 7.5 c_{ext} 7.5

Cytoplasm

σ_{cp} 0.533 S/m

ϵ_{cp} 71

Cell membrane

Classical Model Convert Electrical Model

th_{cm} 0 nm OK

σ_{cm} S/m

ϵ_{cm}

G_{cm} 0 S/m²

C_{cm} 8.5 mF/m²

Search

Criteria

Name:

Author:

Title:

Journal:

Year:

Results

Name	Type	Author	Title	Journal	Year
Polystyrene bead	Homogene...	Arnold, W. M., Schwa...	Surface Conductance and Other P...	Journal of Physical C...	1987
Cell with membrane	Single-shell	Fuhr, G., Glasser, H., ...	Cell manipulation and cultivation ...	Biochimica et Biophy...	1997
Red Blood Cell	Single-shell	Gascoyne, P., Sataya...	Microfluidic approaches to malari...	Acta Tropica	2004
Jurkat cell	Single-shell	Reichle, C., Schnelle, ...	A new microsystem for automate...	Biochimica Et Biophy...	2000
HEK 293 cell line	Single-shell	Zimmermann, D., Kle...	A combined patch-clamp and ele...	Journal of Membrane...	2008
Friend murine erythr...	Single-shell	Wang, X. B., Huang, Y...	Dielectrophoretic manipulation of...	Ieee Transactions on...	1997
Mouse myeloma SP2 ...	Single-shell	Mahaworasilpa, T. L.,...	Forces on Biological Cells Due to ...	Biochimica Et Biophy...	1994
Mouse myeloma SP2 ...	Single-shell	Mahaworasilpa, T. L.,...	Forces on Biological Cells Due to ...	Biochimica Et Biophy...	1994
Human chronic myel...	Single-shell	Mahaworasilpa, T. L.,...	Forces on Biological Cells Due to ...	Biochimica Et Biophy...	1994
Human chronic myel...	Single-shell	Mahaworasilpa, T. L.,...	Forces on Biological Cells Due to ...	Biochimica Et Biophy...	1994
Human breast cance...	Single-shell	Wang, X. B., Huang, Y...	Dielectrophoretic manipulation of...	Biophysical Journal	1997
Human red cell	Single-shell	Gimsa, J. & Wachner, ...	A unified resistor-capacitor mod...	Biophysical Journal	1998
Uncleaved frog (Xen...	Single-shell	Asami, K. & Irimajiri, ...	Dielectrospectroscopic monitorin...	Physics in Medicine ...	2000
Chlorella cell	Single-shell	Ogata, S., Yasukawa, ...	Dielectrophoretic manipulation of...	Bioelectrochemistry	2003
Human carcinoma (...)	Single-shell	Jen, C. P. & Chen, T. W.	Selective trapping of live and dea...	Biomedical Microdev...	2009
MCF10A	Single-shell	Henslee, E. A., Sano, ...	Selective concentration of human ...	Electrophoresis	2011
MCF7	Single-shell	Henslee, E. A., Sano, ...	Selective concentration of human ...	Electrophoresis	2011
MDA-MB-231	Single-shell	Henslee, E. A., Sano, ...	Selective concentration of human ...	Electrophoresis	2011
Uninfected Baby Ha...	Single-shell	Archer, S., Morgan, ...	Electrorotation studies of baby ha...	Biophysical Journal	1999
HSV-1-infected Baby...	Single-shell	Archer, S., Morgan, ...	Electrorotation studies of baby ha...	Biophysical Journal	1999
White Blood cell	Single-shell	Lannin, T., Su, W. W., ...	Automated electrorotation shows ...	Biomicrofluidics	2016
U937 (Lymphoma cell)	Single-shell	Lannin, T., Su, W. W., ...	Automated electrorotation shows...	Biomicrofluidics	2016
PANC1 (Pancreatic c...	Single-shell	Lannin, T., Su, W. W., ...	Automated electrorotation shows...	Biomicrofluidics	2016
Serum-starved PANC1	Single-shell	Lannin, T., Su, W. W., ...	Automated electrorotation shows...	Biomicrofluidics	2016
EMT-induced PANC1	Single-shell	Lannin, T., Su, W. W., ...	Automated electrorotation shows...	Biomicrofluidics	2016
BxPC3 (Pancreatic ca...	Single-shell	Lannin, T., Su, W. W., ...	Automated electrorotation shows...	Biomicrofluidics	2016
Serum starved BxPC3	Single-shell	Lannin, T., Su, W. W., ...	Automated electrorotation shows...	Biomicrofluidics	2016

Sweep σ_m (S/m) nb_{points} 10 Log min 1E-3 max 1.6 Calculate

Close

